Available online at www.sciencedirect.com
ScienceDirect
Acta Biomaterialia 4 (2008) 2008–2015
Acta BIOMATERIALIA
www.elsevier.com/locate/actabiomat

Influence of aggressive ions on the degradation behavior of biomedical magnesium alloy in physiological environment

Yunchang Xin [a,b], Kaifu Huo [a,c], Hu Tao [a], Guoyi Tang [b], Paul K. Chu [a,*]

[a] Department of Physics and Materials Science, City University of Hong Kong, Tat Chee Avenue, Kowloon, Hong Kong, China
[b] Advanced Materials Institute, Tsinghua University, Shenzhen Graduate School, Shenzhen 518055, China
[c] Hubei Province Key Laboratory of Refractories and Ceramics, College of Materials and Metallurgy, Wuhan University of Science and Technology, Wuhan 430081, China

Received 10 December 2007; received in revised form 10 May 2008; accepted 14 May 2008
Available online 11 June 2008

Abstract

Various electrochemical approaches, including potentiodynamic polarization, open circuit potential evolution and electrochemical impedance spectroscopy (EIS), are employed to investigate the degradation behavior of biomedical magnesium alloy under the influence of aggressive ions, such as chloride, phosphate, carbonate and sulfate, in a physiological environment. The synergetic effects and mutual influence of these ions on the degradation behavior of Mg are revealed. Our results demonstrate that chloride ions can induce porous pitting corrosion. In the presence of phosphates, the corrosion rate decreases and the formation of pitting corrosion is significantly delayed due to precipitation of magnesium phosphate. Hydrogen carbonate ions are observed to stimulate the corrosion of magnesium alloy during the early immersion stage but they can also induce rapid passivation on the surface. This surface passivation behavior mainly results from the fast precipitation of magnesium carbonate in the corrosion product layer that can subsequently inhibit pitting corrosion completely. Sulfate ions are also found to stimulate magnesium dissolution. These results improve our understanding on the degradation mechanism of surgical magnesium in the physiological environment.

Keywords: Magnesium alloys; Biomaterial; Degradation; Aggressive ions

1. Introduction

Stainless steels, cobalt-based alloys and titanium alloys are widely studied and applied clinically in hard tissue implants, especially in load-bearing applications, due to their high strength, ductility and good corrosion resistance. However, they cannot degrade spontaneously and a second surgical procedure is usually needed to remove the metal implants from the body after the tissues have completely healed. Repeated surgery increases the cost as well as patient morbidity. In this respect, biodegradable magnesium-based alloys can be a potential solution. Many clinical cases as well as in vivo and in vitro assessments have demonstrated that magnesium alloys possess good biocompatibility [1–3]. Some studies have also shown that the dissolved magnesium ions may promote bone cell attachment and tissue growth on the implants [4–6]. Unfortunately, pure magnesium and its alloys corrode too quickly at physiological pH (7.4–7.2), as well as in physiological media containing high concentrations of aggressive ions, thereby losing mechanical integrity before tissues have sufficient time to heal [1,3,7,8]. This has become the main limitations in clinical applications. The fast degradation rates of Mg alloy are generally considered to result from aggressive ions in the physiological environment, such as chlorides, phosphates, carbonates and sulfates. The aggressive behavior of chloride ions to Mg alloys has been widely investigated and it is generally accepted that chloride ions can transform the protective $MgO/Mg(OH)_2$ into soluble $MgCl_2$

* Corresponding author. Tel.: +852 27887724; fax: +852 27889549.
E-mail address: paul.chu@cityu.edu.hk (P.K. Chu).

1742-7061/$ - see front matter © 2008 Acta Materialia Inc. Published by Elsevier Ltd. All rights reserved.
doi:10.1016/j.actbio.2008.05.014

[9], thus accelerating magnesium dissolution. Phosphates, carbonates and sulfates in the physiological environment may also attack magnesium. However, their influences have rarely been systematically investigated. In addition, the synergetic effect and mutual influence of these ions on the degradation behavior of Mg are not well understood. Electrochemical approaches, such as the potentiodynamic polarization test, open circuit potential evolution and the electrochemical impedance spectrum (EIS), have been widely employed to investigate the corrosion process of alloys, and they are powerful tools to deduce the corrosion mechanism involved [10–12]. However, there have been few reports to date investigating the corrosion mechanism of magnesium alloys in a physiological environment by systematic electrochemical approaches.

In this work, phosphate, carbonate and sulfate ions with the same concentrations as in human body fluid were introduced separately into a sodium chloride solution. Electrochemical approaches including potentiodynamic polarization, open circuit potential evolution and EIS were employed to investigate the degradation behavior of Mg alloys in the solutions containing these ions. In conjunction with scanning electron microscopy (SEM) and Fourier transform infrared (FTIR) characterization, the synergetic effects and mutual influence of the different ions on the degradation behavior of magnesium were systematically investigated and analyzed. The results show that phosphate ions can slow down the corrosion rates significantly, and that carbonate ions can induce surface passivation and totally inhibit pitting corrosion induced by chloride ions. Also, sulfate ions stimulate the corrosion of magnesium. Our results aid our understanding of the degradation mechanism of surgical magnesium in a physiological environment.

2. Experimental

2.1. Sample preparation

Commercial die-cast AZ91 Mg alloys purchased from YiHo Corporation, Shenzhen, China were used. The dimensions of the samples used in the experiments were 15 mm × 15 mm × 3 mm. They were ground with No. 4000 waterproof diamond paper, polished and ultrasonically cleaned in alcohol. Four types of solutions were prepared using NaCl, $NaHCO_3$, K_2HPO_4 and Na_2SO_4. The concentrations of the chloride, phosphate, carbonate and sulfate ions in the four solutions mimic those in human body fluids [13] and are listed in Table 1.

2.2. SEM and FTIR

The samples after immersion for 7 days were taken out of the solutions and ultrasonically cleaned in distilled water. The surface morphology of the samples was observed by SEM. FTIR from 4000 to 400 cm^{-1} was also conducted to identify the functional groups in the corrosion products.

2.3. Degradation rate measurement

The volume of emitted hydrogen during immersion is related to the dissolution of magnesium:

$$Mg + 2H_2O \rightarrow Mg^{2+} + 2OH^- + H_2 \quad (1)$$

The corrosion products do not influence the relationship between hydrogen evolution and magnesium dissolution. The degradation rate of magnesium can thus be monitored by the evolved hydrogen volume, and this method is reliable, easy to implement and not prone to errors inherent in the weight loss method [9]. In addition, this technique has the advantage that variations in the degradation rates can be monitored by the hydrogen evolution rates, allowing the study of the degradation rate variation vs. exposure time. The samples were soaked in 200 ml solutions for 7 days at an ambient temperature of 37 ± 0.5 °C. It has been verified that the dissolved oxygen does not influence the result of the measurements [9] and thus our experiments were carried without deaeration. The emitted hydrogen volumes were measured as a function of immersion time.

2.4. Electrochemical tests

The electrochemical corrosion behavior of the AZ91 magnesium alloy was investigated in the four solutions by potentiodynamic polarization tests, the open circuit potential evolution (E_{corr}–t) and EIS using Gamry Reference 600. A three-electrode cell with the sample as the working electrode, calomel electrode as the reference electrode and platinum electrode as the counter electrode were used. As magnesium reacted in the solution quickly, the potentiodynamic polarization test commenced as soon as the samples were soaked in the solution. A scanning rate of 1 mV s^{-1} was used in the potentiodynamic polarization test. In the E_{corr}–t test, changes in the open circuit potential were monitored as a function of immersion time for about 240 ks. The data were recorded every 120 s. The impedance data were recorded from 100 kHz to 10 mHz with a 10 mV sinu-

Table 1
Ion concentrations in the four solutions

Concentration (mmol l^{-1})	Na^+	K^+	Ca^{2+}	Mg^{2+}	Cl	HPO_4^{-2}	HCO^-_3	SO_4^{-2}
Blood plasma	142.0	5.0	2.5	1.5	103.0	1.0	27.0	0.5
Solution #1	103	–	–	–	103.0	–	–	–
Solution #2	103	2.0	–	–	103.0	1.0	–	–
Solution #3	130	2.0	–	–	103.0	1.0	27.0	–
Solution #4	130.5	2.0	–	–	103.0	1.0	27.0	0.5

soidal perturbing signal at open circuit potential. The lowest frequency was set at 10 mHz in order to reduce the time and potential noise interference. The EIS measurement may be affected by phase shifts from the potentiostat in the high frequency region, and so the upper frequency limit was set at 100 kHz [14]. All the electrochemical tests were carried out at room temperature. Equivalent circuits (EC) were proposed to analyze the obtained EIS spectra. The EIS spectra were fitted with the ZSimpWin software.

3. Results and discussion

3.1. Corrosion morphology

The surface morphology of the samples soaked in the four solutions for 7 days are depicted in Fig. 1. Pitting corrosion takes place on both samples soaked in solutions #1 and #2. Unlike autocatalytic pitting observed on stainless steels, the corrosion pits spread laterally and no deep pitting can be seen. In the high-magnification pictures, many pits (denoted by the arrows) are also observed which are suspected to be the sites with the β phase ($Mg_{17}Al_{12}$). $Mg_{17}Al_{12}$ has a higher standard potential and exhibits a more passive behavior over a wide pH range in chloride solutions than either Al or Mg [9]. Due to selective attack along the β phase networks, they are gradually attacked and peel from the surface forming the pits. Severe corrosion is expected to take place at these sites. Although the by-product of magnesium dissolution, OH^-, can promote precipitation of $Mg(OH)_2$, this corrosion product layer is loose and cannot provide sufficient protection. The chloride ions can transform the formed $Mg(OH)_2$ into more soluble $MgCl_2$, further accelerating the dissolution of the substrate [15]. Corrosion will spread laterally from these sites. This porous corrosion morphology may be the result of the propagation of the pits and subsequent coalescence at the pit fronts. However, no porous pitting corrosion is visually observed on the entire surface of the samples soaked in solutions #3 and #4. Many cracks are discernible, as indicated in Fig. 1, and can probably be attributed to dehydration of the corrosion products in the corroded layer after drying in warm air and the SEM vacuum chamber. These results strongly suggest that the presence of HCO^-_3 in the solutions completely suppresses pitting corrosion on AZ91 magnesium alloy. The reasons will be discussed in more details in subsequent sections.

3.2. FTIR results

X-ray diffraction (XRD) was employed to identify the corrosion products on the samples soaked in the four solutions for 7 days. However, no useful information is acquired except peaks arising from magnesium and the β phase. This may result from the fact that the corrosion

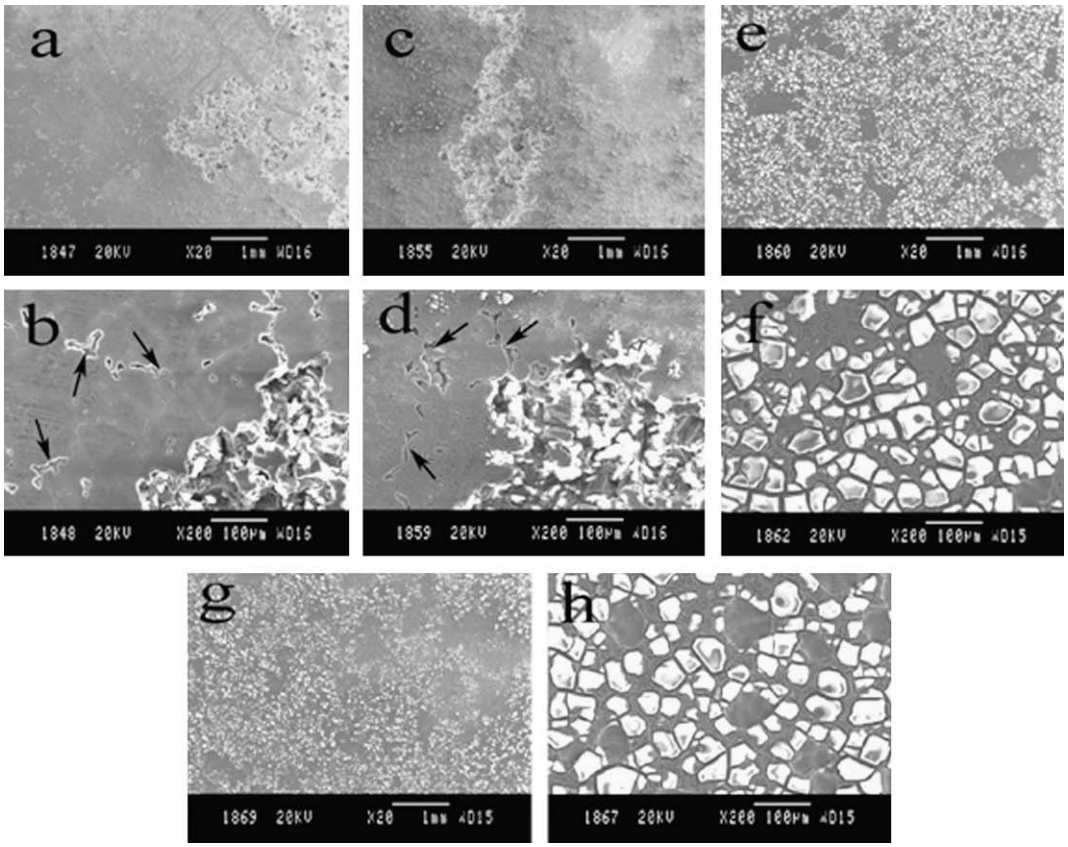

Fig. 1. Surface morphology of AZ91 magnesium samples after immersion in the solutions for 7 days: (a, b) soaked in solution #1; (c, d) soaked in solution #2; (e, f) soaked in solution #3; (g, h) soaked in solution #4.

products are not crystalline. Hence, FTIR was performed to study the corrosion products, and the spectra acquired from samples soaked in the four solutions for 7 days are displayed in Fig. 2. The broad absorption band from 3700 to 2500 cm^{-1} is attributed to the stretching vibration of the hydroxyl group. This broad band stems mainly from water, with strong H bonding inside the structure. In contrast, in the sample soaked in solution #1, a sharp absorption peak at about 3693 cm^{-1} is observed. This higher position peak is related to the free hydroxyl group indicating the presence of magnesium hydroxide [16]. The band at 1640 cm^{-1} arises from H_2O bending vibration. The obvious absorption bands at 1160 and 1040 cm^{-1} correspond to phosphate and the broad band from 1400 to 1550 cm^{-1} originates from carbonate [17]. The bands at 560, 670 and 750 cm^{-1} result from hydroxyl groups mainly in the form of magnesium hydroxide [18]. The 450–550 cm^{-1} band can be ascribed to Mg–O bonding (MgO) [16]. In solution #1, the corrosion products consist mainly of magnesium hydroxide. When magnesium and its alloys are soaked in an aqueous medium, reaction (1) takes place. This reaction leads to an increased pH value and $Mg(OH)_2$ precipitates, forming the corrosion product layer. In the presence of HPO_4^{-2} ions, the insoluble tertiary magnesium phosphate, $Mg_3(PO_4)_2$, tends to precipitate as the corrosion products due to consumption of OH^- produced during magnesium dissolution, as indicated in reaction (1) by the hydroxphosphate ions. Thus, in solution #2, besides magnesium hydroxides, insoluble magnesium phosphates are present in the corrosion product layer. The corrosion products after immersion in solutions #3 and #4 are similar and include magnesium carbonate, magnesium phosphate and magnesium oxide. Similarly, magnesium dissolution results in higher pH values and when the pH of the solution reaches about 9.3, $MgCO_3$ will precipitate on the surface [20].

3.3. Degradation rates

The hydrogen evolution rates that are related to the magnesium dissolution rates are plotted as a function of immersion time in Fig. 3. The degradation rate of the sample in solution #1 diminishes slowly during the first 36 h and then stabilizes subsequently. When the sample is exposed to the corrosion medium, chemical dissolution and electrolyte penetration result in spontaneous corrosion on the entire surface leading to fast degradation rates of the magnesium surface. One by-product of magnesium dissolution is OH^-, which can raise localized corrosion and stabilize the corrosion product ($Mg(OH)_2$). As immersion proceeds, the thickness of the corrosion product layer increases and the corrosion rate decrease gradually. When an equilibrium between dissolution and formation of corrosion products is established, the corrosion rate stabilizes. However, this $Mg(OH)_2$ layer is loose and cannot provide sufficient protection. In addition, the chloride ions on the surface can transform the formed $Mg(OH)_2$ into soluble $MgCl_2$ [9]. Dissolution of $Mg(OH)_2$ makes the surface more active, subsequently decreasing the protected area and causing further dissolution of magnesium. Therefore, the corrosion rate of the sample in solution #1 does not decrease significantly even after a long immersion time. During the first 12 h, the degradation rate in solution #2 is about the same as that in solution #1 and drops dramatically after 24 h. With prolonged exposure, the degradation rates are nearly constant and about half of those in solution #1. The presence of hydrophosphate ions can retard the corrosion rates of magnesium significantly. Unlike $Mg(OH)_2$, the magnesium phosphate in the corrosion product layer is inherently dense and compact, and cannot be affected by the chloride ions [19]. This may be the reason why the corrosion rates in solution #2 are much lower than those in solution #1. However, owing to the low concentration of hydrogen phosphate ions (only 1 mmol l^{-1}), the corrosion rates of magnesium cannot be retarded significantly with less than 24 h of exposure. The initial degradation rates in solutions #3 and #4 are much higher than those in solutions #1 and #2 and drop quickly with expo-

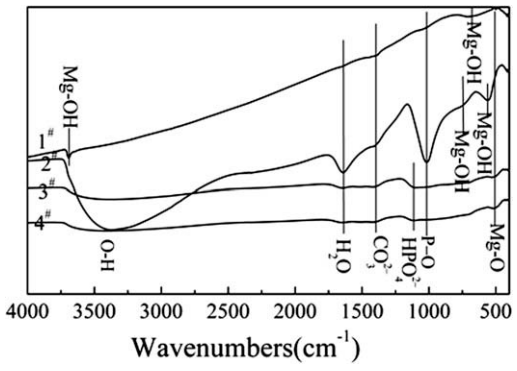

Fig. 2. FTIR spectra of AZ91 magnesium alloys soaked in the four solutions for 7 days.

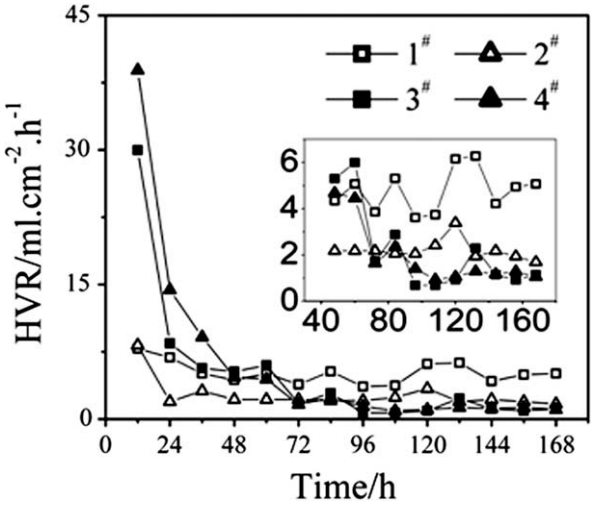

Fig. 3. Hydrogen evolution rates (HVR) from the AZ91 magnesium alloy samples as a function of immersion time in the four solutions.

sure time. The degradation rates stabilize after about 72 h and are similar to each other. It can also be noted that the degradation rates after 96 h exposure in solutions #3 and #4 are even lower than those in solution #2. The consumption of OH^- by HCO^-_3 promotes reaction (1) and accelerates magnesium corrosion as well. Consequently, high corrosion rates of the magnesium alloys during early immersion are observed. However, the by-product of magnesium dissolution is OH^-, which leads to a local increase in pH. The high pH accelerates the precipitation of magnesium phosphate and carbonate, and also stabilizes the magnesium hydroxide. In addition, HCO^-_3 can transform $Mg(OH)_2$ into the more stable giorgiosite ($Mg_5(CO_3)_4(OH)_25H_2O$) [21]. The multiple protection effects offered by magnesium phosphate and carbonate may be the reason for the lower corrosion rates observed in solutions #3 and #4 compared to those in solution #2 after 96 h of immersion. As the protective layer thickens, the corrosion rates of the substrate gradually diminish, eventually attaining constant values. The degradation rates in solution #4 are higher than those in solution #3 during the first 72 h, suggesting that the sulfate ions in solution #4 also aggressively attack magnesium.

3.4. Electrochemical behavior

Representative potentiodynamic polarization curves acquired from samples immersed in the four solutions are displayed in Fig. 4. The Tafel fit is employed to analyze the polarization curves. The samples exhibit low corrosion potentials of about −1774 and −1789 mV in solutions #3 and #4, respectively. The corrosion potentials of the samples in solutions #1 and #2 are about −1530 and −1518 mV, which are nearly the same and about 250 mV nobler than those in solutions #3 and #4. Furthermore, the corrosion current densities in solutions #3 and #4 are much higher than those in solutions #1 and #2. However, a brief passivation region appears in the curves acquired from the samples soaked in solutions #3 and #4. As mentioned above, hydrocarbonate can accelerate the corrosion rate significantly during the early immersion stage, giving rise to more negative potentials. The higher pH values lead to the rapid formation of magnesium carbonate as well as magnesium phosphate on the surface, resulting in surface passivation. When the β phase comes off the surface, fast passivation at these sites occurs quickly, and hence corrosion propagation is limited. The presence of surface passivation is probably the reason for the absence of porous pitting corrosion in the sample soaked in solutions #3 and #4.

The typical E_{corr}–t curves of the AZ91 magnesium alloys exposed to the four solutions are shown in Fig. 5. At first, the potential of the sample in solution #1 increases rapidly, but drops quickly thereafter. Subsequently, the corrosion potential experiences a short anodic polarization. A sharp drop in the potential occurs at about 18 ks, indicating the occurrence of pitting corrosion, and intensive fluctuations in the corrosion potential appear during the subsequent immersion. The fluctuations reveal spreading of the corrosion pits and/or formation of new pits [14]. The potential of the sample immersed in solution #2 increases gradually at first. There is then an abrupt drop at about 150 ks, implying the emergence of the first corrosion pits. The initial increase in the corrosion potential also clearly results from the precipitation of the protective magnesium phosphate as well as magnesium hydroxide. It should be noted that pitting corrosion occurrence is significantly delayed, suggesting that phosphate ions can suppress pitting corrosion on magnesium. Although porous pitting corrosion is also present, this may be attributed to the low concentration of phosphate ions in solution #2, and fast passivation cannot occur after pit formation. The curves obtained from the samples immersed in solutions #3 and #4 are quite similar. From the beginning, the potentials shift to the nobler direction gradually and smoothly. No large fluctuations in the corrosion potentials can be observed during the entire exposure duration, indicating a general corrosion process in solutions #3 and #4. The increase in the corrosion potentials are also related to the gradually enhanced protection offered by the corrosion product layer. The above

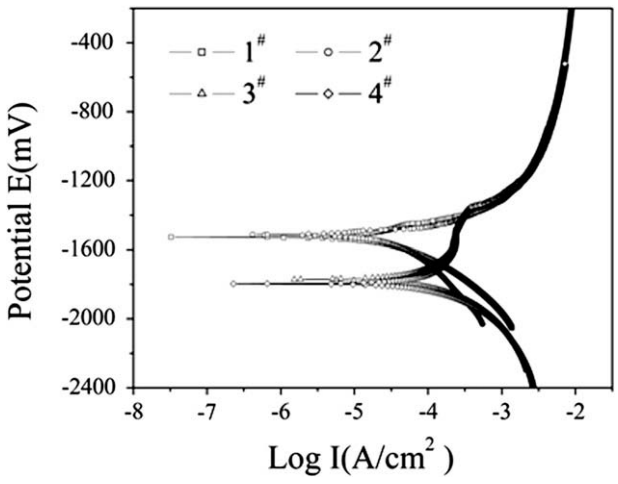

Fig. 4. Representative potentiodynamic polarization curves of AZ91 magnesium alloy sample soaked in the four solutions.

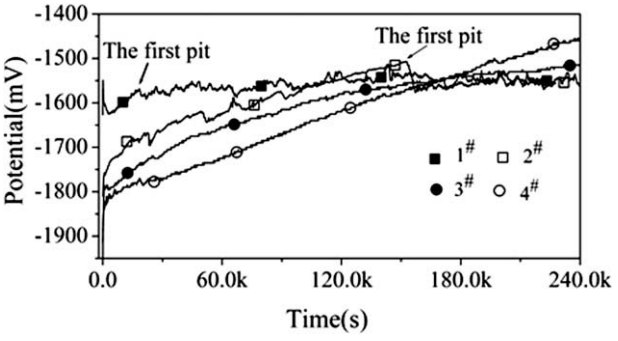

Fig. 5. Open circuit potentials evolution of the AZ91 magnesium alloy samples immersed in the four solutions as a function of exposure time.

results imply that formation of Mg carbonates may have a large effect on the suppression of pitting corrosion, and the presence of carbonates totally inhibit pitting corrosion.

EIS is a powerful technique with which to study the electrochemical corrosion process on metals. When an excitation signal with a small amplitude is applied, the response depends on the electrode kinetics. It usually consists of several different sub-processes, including mass transfer and charge transfer. By analyzing these responses, the individual sub-process can be deduced [11]. The EIS spectra acquired from the AZ91 magnesium alloys soaked in the four solutions for about 0.5 h are presented in Fig. 6. In the curves obtained from the samples in solutions #1 and #2, two time constants are observed: one capacitive arc in the high frequency region and one capacitive arc in the low frequency region. Generally the capacitive arcs result from charge transfer and film effects, as well as mass transportation. The curves obtained in solutions #3 and #4 exhibit a capacitive loop in the high frequency region, a capacitive loop in the middle frequency region and a pseudo-inductive loop in the low frequency region. The presence of the inductive loops in spectra #3 and #4 indicates two surface states. Considering the presence of the passivation region in the potentiodynamic polarization curves, the two surface states are the active region and the passive region. The EIS spectra acquired after immersion in the four solutions for 6 h are shown in Fig. 7. The spectrum obtained from the sample in solution #1 contains two enlarged capacitive arcs. In the spectrum obtained from the sample in solution #2, the capacitive arc in the high frequency range is enlarged. However, the capacitive arc in the low frequency range is nearly invisible. In the spectra acquired from the samples in solutions #3 and #4, one capacitive arc at high frequency and one capacitive arc at low frequency are seen. Both capacitive arcs are also enlarged. The inductive loop becomes almost invisible and the diminishing inductive loop indicates an increasing passivation area. As shown in Fig. 8, after 24 h immersion, the system in solution #1 still shows two

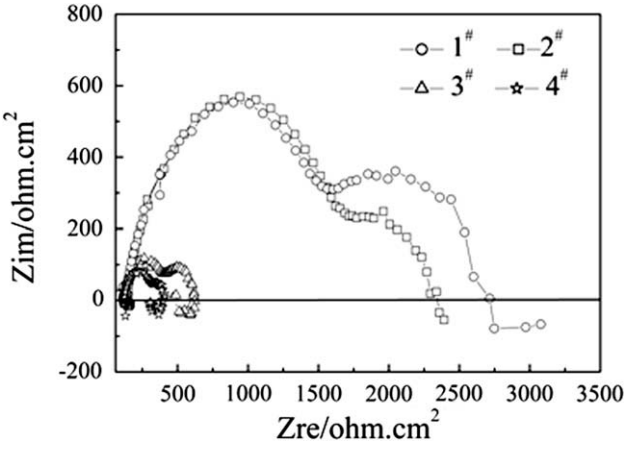

Fig. 7. Representative EIS spectra of AZ91 magnesium alloy soaked in the four solutions for 6 h.

larger capacitive arcs. No obvious changes in the spectrum taken from the sample in solution #2 can be observed. In solutions #3 and #4, the capacitive arcs are larger to some extent. In addition, the inductive loops in the spectra obtained in solutions #3 and #4 vanish almost entirely, implying only one dominated surface state, which is the passive state.

EC that not only match the physical structure but also create similar spectra as test spectra are proposed and shown in Fig. 9 with (a) being the analysis of the EIS spectra without inductive loops and (b) being the fits of the spectra with inductive loops. C_f, one of the constant phase element (CPE) components, represents the capacitance of the corrosion products layer and R_f is the corresponding layer resistance. C_{dl}, another component of CPE, expresses the capacitance of the double layer at vulnerable regions. R_t is the charge transfer resistance related to the electrochemical reaction in the same region. R_s is the solution resistance between the reference and working electrodes, but has nothing to do with the electrode process. Its value depends on the conductivity of the test medium and the

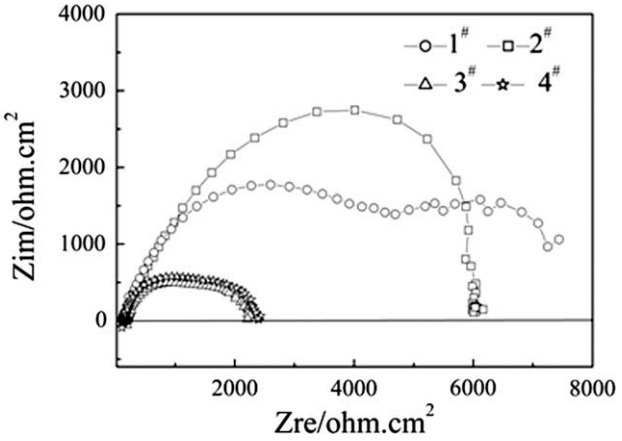

Fig. 6. Representative EIS spectra of AZ91 magnesium alloy soaked in the four solutions for 0.5 h.

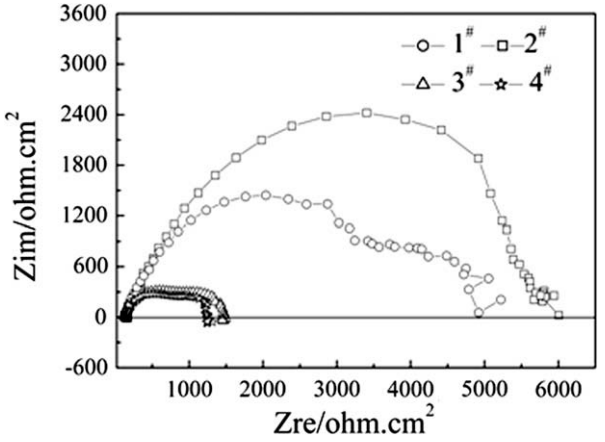

Fig. 8. Representative EIS spectra of AZ91 magnesium alloy soaked in the four solutions for 24 h.

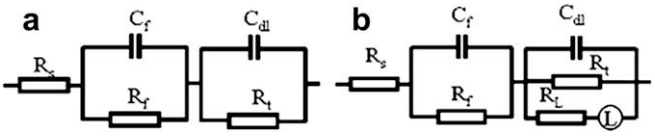

Fig. 9. EC for analysis EIS spectra of AZ91 magnesium alloy soaked in the four test solutions for different durations: (a) for spectra without inductive loop; (b) for spectra with inductive loop.

geometry of the cell [14]. As usual, R_s is placed in series with other elements of the circuit. R_L and L originate from the inductive loops in the EIS spectra. The fitted EIS results of the samples soaked in solutions #1–#4 as a function of immersion time are listed in Tables 2–5, respectively. For sample in solution #1, C_f decreases dramatically after 6 h immersion. With prolonged immersion durations, no significant decrease is observed. Both R_f and R_t increase greatly after 6 h exposure, and at the end of 24 h, only a little increase is observed. These results reveal that the corrosion rates of the samples decrease significantly during the first 6 h. This may indicate the dramatically decreased fresh/active surface area due to the formation of corrosion products on the surface. After 6 h, the corrosion product layer thickens, leading to a slow decrease in the corrosion rates. The capacitance of the double layer, C_{dl}, that shows the typical metal/solution system, which varies from 10 to 100 μF [14] with continuous immersion, decreases slightly. Here, m and n are indices of the dispersion effects of the CPE components, C_f and C_{dl}, respectively representing their deviations from the ideal capacitance due to the inhomogeneity and roughness of the electrode on the microscale. The values of m and n are always $0 < m, n < 1$. It is obvious that the values of m and n in our experiments are in this range. In solution #2, no obvious changes in C_f or R_f after 6 h of exposure can be observed. However, R_f and R_t increase significantly and C_f decreases slightly after 24 h immersion, indicating the progressive enhancement of protection from the corrosion product layer. Considering the consumption of OH^- by hydrophosphate ions during early immersion, the formation of corrosion product as $Mg(OH)_2$ is suppressed and thus C_f and R_f change very little. Owing to the low concentration of hydrophosphate ions, after a long exposure, the pH value increases progressively and the corrosion products gradually precipitate on the surface, leading to greatly enhanced values in both R_f and R_t; C_f also decreases. C_{dl}, m and n are in the typical range. With regard to solutions #3 and #4, similar variations in the values of the components are observed. Both R_f and R_t increase gradually with immersion time, while C_f decreases gradually with increased exposure dura-

Table 2
EIS fitted results of sample in solution #1 for 0.5, 6 and 24 h

Time (h)	R_s (Ω cm^2)	C_f (10^{-3}F cm^{-2})	m	R_f (Ω cm^2)	C_{dl} (10^{-6}F cm^{-2})	n	R_t (Ω cm^2)
0.5	134	2.87	0.959	542	28.14	0.787	1592
6	139	0.038	0.800	710	20.15	0.930	4800
24	144	0.031	0.781	914	20.03	0.990	5062

Table 3
EIS fitted results of sample in solution #2 for 0.5, 6 and 24 h

Time (h)	R_s (Ω cm^2)	C_f (10^{-3}F cm^{-2})	m	R_f (Ω cm^2)	C_{dl} (10^{-6}F cm^{-2})	n	R_t (Ω cm^2)
0.5	130	1.60	0.942	909	29.59	0.785	1513
6	146	2.28	0.996	1170	34.25	0.800	3712
24	151	0.7	0.774	3870	20.03	0.830	4111

Table 4
EIS fitted results of sample in solution #3 for 0.5, 6 and 24 h

Time (h)	R_s (Ω cm^2)	C_f (10^{-3}F cm^{-2})	m	R_f (Ω cm^2)	C_{dl} (10^{-6}F cm^{-2})	n	R_t (Ω cm^2)
0.5	122	1.46	0.543	423	24.14	0.866	229
6	133	0.54	0.771	782	40.72	0.865	609
24	167	0.48	0.565	1161	60.58	0.860	932

Table 5
EIS fitted results of sample in solution #4 for 0.5, 6 and 24 h

Time (h)	R_s (Ω cm^2)	C_f (10^{-3}F cm^{-2})	m	R_f (Ω cm^2)	C_{dl} (10^{-6}F cm^{-2})	n	R_t (Ω cm^2)
0.5	121	1.31	0.737	122	19.14	0.920	176
6	129	0.64	0.806	581	42.2	0.845	599
24	124	0.55	0.810	1136	55.21	0.848	1142

tion. All these changes indicate the gradually enhanced protection offered by the precipitated corrosion products.

4. Conclusion

The effects of aggressive ions with concentrations similar to those in the physiological environment on the degradation behaviour of AZ91 magnesium alloys have been systematically studied for the first time. Chloride ions induce porous pitting corrosion on the magnesium alloys. Phosphate ions can retard the corrosion rate effectively and delay the emergence of pitting corrosion. During early immersion, carbonate ions promote the dissolution of magnesium. However, they induce rapid surface passivation due to precipitation of magnesium carbonate, which totally suppresses pitting corrosion. Sulphate ions also attack magnesium. Our results provide a better understanding of the degradation mechanism of magnesium alloy in the physiological environment and should be helpful to clinical applications of biomedical magnesium alloys.

Acknowledgements

The Project was supported by a City University of Hong Kong Applied Research Grant (ARG, No. 9667002), the Key Grant Project of Educational Commission of Hubei Province (Z200711001) and the Key Project of Chinese Ministry of Education (No. 208087).

References

[1] McBride ED. Absorbable metal in bone surgery. J Am Med Assoc 1938;111:2464–7.
[2] Vormann J. Magnesium: nutrition and metabolism. Mol Aspects Med 2003;24:27–37.
[3] Witte F, Kaese V, Haferkamp H, Switzer E, Meyer-Lindenberg A, Wirth CJ, et al. In vivo corrosion of four magnesium alloys and the associated bone response. Biomaterials 2005;26:3557–63.
[4] Zreiqat H, Howlett CR, Zannettino A, Evans P, Schulze-Tanzil G, Knabe C, et al. Mechanisms of magnesium-stimulated adhesion of osteoblastic cells to commonly used orthopaedic implants. J Biomed Mater Res 2002;62:175–84.
[5] Revell PA, Damien E, Zhang XS, Evans P, Howlett CR. The effect of magnesium ions on bone bonding to hydroxyapatite. Key Eng Mater 2004;254:447–50.
[6] Yamasaki Y, Yoshida Y, Okazaki M, Shimazu A, Kubo T, Akagawa Y, et al. Action of FG–$MgCO_3$ Ap–collagen composite in promoting bone formation. Biomaterials 2003;24:4913–20.
[7] Witte F, Fischer J, Nellesen J, Crostack HA, Kaese V, Pisch A, et al. In vitro and in vivo corrosion measurements of magnesium alloys. Biomaterials 2006;27:1013–8.
[8] Staiger MP, Pietak AM, Huadmai J, Dias G. Magnesium and its alloys as orthopedic biomaterials: a review. Biomaterials 2006;27:1728–34.
[9] Song GL, Atrens A. Understanding magnesium corrosion – a framework for improved alloy performance. Adv Eng Mater 2003;5:837–58.
[10] Mathieu S, Rapin C, Steinmetz J, Steinmetz P. A corrosion study of the main constituent phases of AZ91 magnesium alloys. Corros Sci 2003;45:2741–55.
[11] Song GL, Atrens A, John DST, Wu X, Nairn J. The anodic dissolution of magnesium in chloride and sulphate solutions. Corros Sci 1997;39:1981–2004.
[12] Baril G, Galicia G, Deslouis C, Pebere N, Ttibollet B, Vivier V. An impedance investigation of the mechanism of pure magnesium corrosion in sodium sulfate solutions. J Electrochem Soc 2007;154:C108–13.
[13] Cho SB, Nakanishi K, Kokubo T, Soga N, Ohtsuki C, Nakamura T, et al. Dependence of apatite formation on silica-gel on its structure – effect of heat-treatment. J Am Ceram Soc 1995;78:1769–74.
[14] Zhang YJ, Yan CW, Wang FH, Li WF. Electrochemical behavior of anodized Mg alloy in chloride containing aqueous solution. Corros Sci 2005;47:2816–31.
[15] Song GL, Andrej A. Corrosion mechanisms of magnesium alloys. Adv Eng Mater 1999;1:11–33.
[16] Tongamp W, Zhang QW, Saito F. Preparation of meixnerite (Mg–Al–OH) type layered double hydroxide by a mechanochemical route. J Mater Sci 2007;42:9210–5.
[17] Weng J, Liu Q, Wolke JGC, Zhang XD, deGroot K. Formation and characteristics of the apatite layer on plasma-sprayed hydroxyapatite coatings in simulated body fluid. Biomaterials 1997;18:1027–35.
[18] Shao CL, Guan HY, Liu YC, Mu RX. MgO nanofibres via an electrospinning technique. J Mater Sci 2006;41:3821–4.
[19] Morks MF. Magnesium phosphate treatment for steel. Mater Lett 2004;58:3316–9.
[20] Gao JC, Li LC, Wang Y. Surface modification on magnesium by alkali-heat-treatment and its corrosion behaviors in SBF. Chinese J Nonferrous Met 2004;14:1508–13.
[21] Lindstrom R, Johansson LG, Thompson GE, Skeldon P, Svensson JE. Corrosion of magnesium in humid air. Corros Sci 2004;46:1141–58.